Sparse Echo Reconstruction of Micro-motion Targets Under the Joint Constraints of Low-rank and Periodic Consistency

Mingming Jin*, Jun Wang†, Shaoming Wei*, Peng Lei*
* Beihang University, Beijing, China
E-mail: jimmyking@buaa.edu.cn, shaoming.wei@buaa.edu.cn, buaaray@gmail.com
†Hangzhou innovation institute of Beihang university, Hangzhou, China
E-mail: wangj203@buaa.edu.cn

***Abstract*—In practical scenarios, affected by electronic countermeasures or multitasking requirements, radar echoes from the same micro-motion target inevitably exhibit sparsity. To solve this problem, this paper proposes a sparse echo reconstruction method for micro-motion targets based on joint constraints of low-rank property and periodic consistency, aiming to enhance reconstruction performance. First, the wideband sparse echo signal model under random missing sampling (RMS) for micro-motion targets is established; then, inspired by the concept of matrix completion (MC), the "periodic consistency" constraint is introduced into the objective function, constructing an optimization model for echo signal reconstruction based on the low-rank property. Meanwhile, the alternating direction method of multipliers (ADMM) reconstructs echoes through alternate iterations and gradual optimization. Finally, simulation experiments validate the effectiveness of the proposed algorithm.**

I. INTRODUCTION

The micro-motions of space targets induce complex modulation effects on radar echo signals, also known as the micro-Doppler (m-D) effect [1]. The m-D effect contains information about the target's shape, size, and scattering characteristics, and is widely applied in both civilian and military fields [2][3]. Among various forms of micro-motion, precession is capable of distinguishing different space targets and has been extensively studied. However, existing studies are mostly limited to full-aperture echo data, and sparse signal processing for micro-motion targets is still insufficient.

Sparse observations disrupt the coherence among echo signals from micro-motion targets, posing a critical challenge in practical engineering applications. On one hand, when full-aperture observation samples are contaminated by passive interference or radar malfunctions, some samples must be discarded, thus compromising the integrity of the echo signals. On the other hand, multifunctional requirements such as radar tracking and imaging prevent continuous observation of the same micro-motion target, leading to sparse echo signals. To address the above problems, sparse signal processing techniques based on compressed sensing (CS) have been proposed successively. In [4], orthogonal matching pursuit (MP) algorithm reconstructs cone-shaped target echoes, and preliminary verification with experimental data confirmed the effectiveness of sparse recovery methods. In [5], a Smoothed L0-norm (SL0) algorithm was used to recover echo signals with block-missing samples, enabling sparse ISAR imaging in short-time observation. However, for most CS algorithms, discrete dictionaries inevitably lead to grid discretization, known as the "off-grid" problem, causing model mismatch and reconstruction errors.

Recently, as a two-dimensional extension of CS, matrix completion (MC) theory has developed rapidly in the field of sparse signal reconstruction. By leveraging low-rank constraints, MC can recover missing elements of a matrix under certain conditions. Reference [6] proposed an MC method based on the Hankel matrix, which improved ISAR imaging performance in sparse scenarios. In [7], MC addressed the interference suppression problem in FMCW radar signals, enabling denoising and the recovery of full-aperture echo signals. It is worth noting that research on the application of MC to sparse signals of micro-motion targets remains rarely reported.

To address the above challenges and inspired by MC methods, we formulate sparse echo reconstruction for micro-motion targets as a low-rank matrix optimization problem. Unlike other scenarios, the micro-motion of space targets exhibits typical periodicity. To leverage this property and enhance the effectiveness of sparse reconstruction, this paper introduces "periodic consistency" to facilitate echo signal recovery. Finally, the alternative direction method of multipliers (ADMM) algorithm is employed to solve the objective function through multiple alternating iterations, gradually reconstructing the sparse echo signals.

The rest of this paper is organized as follows. Section II establishes the sparse signal model of wideband echoes from

979-8-3315-7206-8/25/$31.00

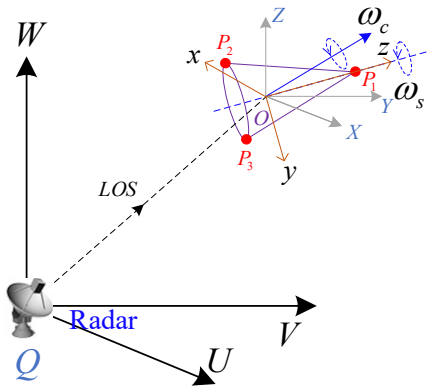

Fig. 1 Geometric model of the micro-motion target

micro-motion targets. Section III describes the proposed sparse echo reconstruction method based on joint low-rank and periodic consistency constraints. In Section IV, the effectiveness and performance of the proposed algorithm are analyzed via simulated data. Finally, some conclusions are drawn in section V.

II. Signal Model

The spatial geometry of a wideband radar and a micro-motion target is shown in Fig. 1. According to the Geometrical Theory of Diffraction (GTD), the electromagnetic scattering of the target can be considered as the synthesis of local electromagnetic scattering from each scattering center. Assuming that the radar transmits a linear frequency modulated (LFM) signal, the "dechirp" processing is performed on the echo signal. For a target with K scattering centers, the baseband signal can be expressed as [6]

$$\begin{aligned} & s\left(\hat{t},t_n\right) \\ & =\sum_{k=1}^{K}\sigma_k\cdot rect\left[\frac{\hat{t}-\frac{2R_k\left(t_n\right)}{c}}{T_p}\right]\cdot\exp\left\{-\frac{j4\pi f_c}{c}\left[R_k\left(t_n\right)-R_{ref}\right]\right\} \\ & \cdot\exp\left\{-\frac{j4\pi\mu}{c}\left[R_k\left(t_n\right)-R_{ref}\right]\left(\hat{t}-\frac{2R_{ref}}{c}\right)\right\} \\ & \cdot\exp\left\{\frac{j4\pi\mu}{c^2}\left[R_k\left(t_n\right)-R_{ref}\right]^2\right\} \end{aligned} \tag{1}$$

where $\hat{t}$ is the fast time and t_n is the show time. c represents the light speed, T_p is the time duration. μ stands for the frequency modulation slope, f_c is the center frequency, and R_{ref} refers to the reference distance. Additionally, $R_k\left(\hat{t},t_n\right)$ indicates the actual distance between the k-th scattering center and the radar at slow time t_n, while σ_k denotes the scattering intensity of the k-th scattering center.

A smooth cone-shaped target typically contains two types of scattering centers [8]: localized scattering centers (LSC, i.e., P_1) and sliding-type scattering centers generated by edge diffraction (SSCE, i.e., P_2, P_3), as illustrated in Fig. 1. The paper mainly analyzes the micro-motion state of the cone target in the precession form, with occlusion effects excluded from observation. ω_c represents the cone rotation angular velocity, and ω_s represents the spin angular velocity. For convenience, the micro-motion distance of scattering centers is defined as $R_{\Delta k}\left(t_n\right)=R_k\left(t_n\right)-R_{ref}$.

For LSC, its micro-motion is predominantly modulated by coning dynamics. According to [2], $R_{\Delta k}$ can be written as

$$R_{\Delta k}\left(t_n\right)=r_s+A_s\sin\left(\omega_c t_n+\varphi_s\right) \tag{2}$$

where r_s, A_s and φ_s are all constants. In (2), the micro-motion distance of the LSC conforms to the law of sinusoidal modulation.

For SSCE, the micro-motion distance is determined not only by coning dynamics, but also by the plane containing the radar line-of-sight (LOS) and the cone axis OP_1. According to [9], $R_{\Delta k}$ is expressed as

$$R_{\Delta k}\left(t_n\right)=h_2\cos\varphi\left(t_n\right)\pm r\sin\varphi\left(t_n\right) \tag{3}$$

where h_2 denotes the distance from the cone centroid O to the base, and r represents the base radius. The angle $\varphi\left(t_n\right)$, defined between the LOS and OP_1 at t_n, can be derived as

$$\cos\varphi\left(t_n\right)=\cos\theta\cos\alpha+\sin\theta\sin\alpha\sin\left(\omega_c t_n-\phi_s\right) \tag{4}$$

where, θ is the precession angle, α signifies the angle between the cone rotation axis and LOS, and ϕ_s denotes the initial phase. For comprehensive derivations of the aforementioned modeling, please refer to [2] and [9].

By integrating (2) to (4), it can be observed that the micro-motion distances of the two types of scattering centers both exhibit periodic modulation, with a period of $T_c=2\pi/\omega_c$. This provides a foundation for the subsequent algorithm.

The above model is based on the full aperture (FA) data, then we introduce the sparse signal model for random missing sampling (RMS). We mainly focus on the RMS situation in the slow time dimension, where the missing samples occur at arbitrary places along the slow-time dimension in the complete dataset [10]. Fig. 2 provides a schematic of the sampling matrix $\mathbf{\Omega}$ corresponding to the RMS. Consider the discrete form of the signal, the echo matrix with M frequency points and N slow-time samples is expressed as

$$\begin{aligned} \mathbf{S}_{\mathrm{FA}} &= \begin{bmatrix} s(1,1) & s(1,2) & \cdots & s(1,N) \\ s(2,1) & s(2,2) & \cdots & s(1,N) \\ \vdots & \vdots & \ddots & \vdots \\ s(M,1) & s(M,2) & \cdots & s(M,N) \end{bmatrix}_{M\times N} \\ &= \begin{bmatrix} s_{\mathrm{f}1} & s_{\mathrm{f}2} & \cdots & s_{\mathrm{f}N} \end{bmatrix} \end{aligned} \tag{5}$$

where each element $s(m,n)$ in $\mathbf{S}_{\mathrm{FA}}$ corresponds to indices $m\in\{1,\cdots,M\}$ and $n\in\{1,\cdots,N\}$. $s_{\mathrm{f}n}$ represents the complete echo signal at the n-th slow time.

Assuming slow-time echo sequences are randomly missing ($Q<N$), and their positions are

$$n_q\in N_Q=\{n_{q1},n_{q2},\ldots,n_{qQ}\}\subset N_F=\{1,2,\ldots,N\} \tag{6}$$

The missing columns in $\mathbf{S}_{\mathrm{FA}}$ (i.e., columns indexed by n_q) are zero-padded to construct the RMS echo matrix $\mathbf{X}$

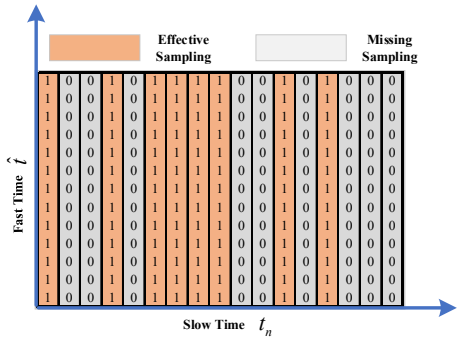

Fig. 2 Random missing sampling (RMS) pattern matrix

$$\mathbf{X}=\mathbf{S}_{\mathrm{FA}}\odot\mathbf{\Omega} \tag{7}$$

where $\odot$ means Hadamard product. The data missing ratio is denoted by $\vartheta=Q/N$. The subsequent section will introduce a reconstruction framework that leverages low-rank properties and periodic similarity constraints to restore the missing echo signals in **X**.

III. Proposed Method

Traditionally, based on the MC, the rank minimization problem can be expressed as

$$\begin{aligned}&\min \operatorname{rank}(\mathbf{X})\\ &\text{s.t. } \mathbf{X}(m,n)=\mathbf{S}(m,n)\quad \forall(m,n)\in\Omega\end{aligned} \tag{8}$$

To further exploit the low-rank property, we transform X into an enhanced Hankel matrix $\mathcal{H}\{\mathbf{X}\}$ for processing

$$\mathcal{H}\{\mathbf{X}\}=\begin{bmatrix}\mathcal{H}\{\mathbf{X}(:,1)\} & \mathcal{H}\{\mathbf{X}(:,2)\} & \cdots & \mathcal{H}\{\mathbf{X}(:,2Q+1)\}\\ \mathcal{H}\{\mathbf{X}(:,1)\} & \mathcal{H}\{\mathbf{X}(:,3)\} & \iddots & \mathcal{H}\{\mathbf{X}(:,2Q+2)\}\\ \vdots & \vdots & \iddots & \\ \mathcal{H}\{\mathbf{X}(:,N-2Q)\} & \mathcal{H}\{\mathbf{X}(:,N-2Q+1)\} & \cdots & \mathcal{H}\{\mathbf{X}(:,N)\}\end{bmatrix} \tag{9}$$

where,

$$\mathcal{H}\{\mathbf{X}(:,n)\}=\begin{bmatrix}\mathbf{X}(1,n) & \mathbf{X}(2,n) & \cdots & \mathbf{X}(2P+1,n)\}\\ \mathbf{X}(2,n) & \mathbf{X}(3,n) & \iddots & \mathbf{X}(2P+2,n)\}\\ \vdots & \vdots & \iddots & \\ \mathbf{X}(M-2P,n) & \mathbf{X}(M-2P+1,n) & \cdots & \mathbf{X}(M,n)\}\end{bmatrix} \tag{10}$$

where, Q and Q are row parameters.

The optimization model for the enhanced Hankel matrix is formulated as

$$\begin{aligned}&\min \operatorname{rank}(\mathcal{H}\{\mathbf{X}\})\\ &\text{s.t. } \mathbf{X}(m,n)=\mathbf{S}(m,n)\quad \forall(m,n)\in\Omega\end{aligned} \tag{11}$$

In order to reduce the computational complexity, we incorporate matrix factorization and the Frobenius norm into the solution process, (11) is rewritten as

$$\begin{aligned}&\min \|\mathbf{U}\|_F^2+\|\mathbf{V}\|_F^2\\ &\text{s.t. } \mathcal{H}\{\mathbf{X}\}=\mathbf{U}\mathbf{V}^H\\ &\quad \mathbf{X}(m,n)=\mathbf{S}(m,n)\quad \forall(m,n)\in\Omega\end{aligned} \tag{12}$$

where $\|\cdot\|_F^2$ denotes the Frobenius norm, and $[\cdot]^H$ denotes the conjugate transpose of the matrix. For **X** under the RMS condition, we accumulate the echo signals corresponding to each slow-time moment by rows to obtain $\mathbf{x}(n)$, and the autocorrelation function of $\mathbf{x}(n)$ is

$$C_{\mathbf{x}}(\tau)=\sum_{n=0}^{N-\tau-1}\mathbf{x}(n)\mathbf{x}^*(n+\tau) \tag{13}$$

Therefore, the delay corresponding to the micro-motion period can be estimated as

$$\begin{aligned}&\hat{T}_{est}=\arg\max_{\tau}\left[\left|C_{\mathbf{x}}(\tau)\right|\right]\\ &s.t.\ \tau>0\\ &\quad \tau \text{ is the delay corresponding to the local maximum}\end{aligned} \tag{14}$$

where, τ is estimated based on the non-zero coordinate positions corresponding to the second-best local maximum of $\left|C_{\mathbf{x}}(\tau)\right|$, and $|\cdot|$ denotes the modulo operator. Using $\hat{T}_{est}$ and (12), we construct the "periodic consistency" constraint, and update the objective function

$$\begin{aligned}&\min \|\mathbf{U}\|_F^2+\|\mathbf{V}\|_F^2+\lambda\|\mathbf{Z}\|_*\\ &\text{s.t. } \mathcal{H}\{\mathbf{X}\}=\mathbf{U}\mathbf{V}^H\\ &\quad \mathbf{X}(m,n)=\mathbf{S}(m,n)\quad \forall(m,n)\in\Omega\\ &\quad \mathbf{Z}=G\{\mathbf{X}\}\end{aligned} \tag{15}$$

$$G\{\mathbf{X}\}=\left[vect\{\mathbf{X}(:,1{:}\hat{T}_{est})\},\ vect\{\mathbf{X}(:,\hat{T}_{est}{+}1{:}2\hat{T}_{est})\},\ \cdots\right] \tag{16}$$

where, λ is the regularization parameter, $\|\cdot\|_*$ denotes the nuclear norm, and $vect\{\cdot\}$ represents stacking columns of a matrix into a vector one after the other. $G\{\cdot\}$ represents the operation of arranging the vectorized block matrix into a new matrix by columns. Obviously, the nuclear norm is used to measure "periodic consistency", which aids in reconstructing the missing elements. To efficiently solve the optimization, the ADMM algorithm is employed. The augmented Lagrange function is defined as

$$\begin{aligned}&L(\mathbf{X},\mathbf{Z},\mathbf{U},\mathbf{V},\mathbf{R}_1,\mathbf{R}_2)=\frac{1}{2}\left(\|\mathbf{U}\|_F^2+\|\mathbf{V}\|_F^2\right)+\lambda\|\mathbf{Z}\|_*\\ &+\frac{\rho_1}{2}\left\|\mathcal{H}\{\mathbf{X}\}-\mathbf{U}\mathbf{V}^H+\mathbf{R}_1\right\|_F^2+\frac{\rho_2}{2}\left\|\mathbf{Z}-G\{\mathbf{X}\}+\mathbf{R}_2\right\|_F^2\end{aligned} \tag{17}$$

where, $\mathbf{R}_1$ and $\mathbf{R}_2$ are the auxiliary variables, and ρ_1 and ρ_2 are penalty coefficients. In the ADMM framework, the variables **X**, **Z**, **U**, **V**, $\mathbf{R}_1$ and $\mathbf{R}_2$ are updated by minimizing the augmented lagrangian function. Specifically, the $(i+1)$-th iteration of the ADMM algorithm can be expressed as

$$\begin{cases}\mathbf{X}^{(i+1)}=\arg\min_{\mathbf{X}}\dfrac{\rho_1}{2}\left\|\mathcal{H}\{\mathbf{X}\}-\mathbf{U}^{(i)}\mathbf{V}^{(i)H}+\mathbf{R}_1{}^{(i)}\right\|_F^2\\ \qquad\qquad +\dfrac{\rho_2}{2}\left\|\mathbf{Z}^{(i)}-G\{\mathbf{X}\}+\mathbf{R}_2{}^{(i)}\right\|_F^2\\ \mathbf{Z}^{(i+1)}=\lambda\|\mathbf{Z}\|_*+\dfrac{\rho_2}{2}\left\|\mathbf{Z}-G\left\{\mathbf{X}^{(i+1)}\right\}+\mathbf{R}_2{}^{(i)}\right\|_F^2\\ \mathbf{U}^{(i+1)}=\arg\min_{\mathbf{U}}\dfrac{1}{2}\|\mathbf{U}\|_F^2+\dfrac{\rho_1}{2}\left\|\mathcal{H}\{\mathbf{X}^{(i+1)}\}-\mathbf{U}\mathbf{V}^{(i)H}+\mathbf{R}_1{}^{(i)}\right\|_F^2\\ \mathbf{V}^{(i+1)}=\arg\min_{\mathbf{V}}\dfrac{1}{2}\|\mathbf{V}\|_F^2+\dfrac{\rho_2}{2}\left\|\mathcal{H}\left\{\mathbf{X}^{(i+1)}\right\}-\mathbf{U}^{(i+1)}\mathbf{V}^H+\mathbf{R}_1{}^{(i)}\right\|_F^2\\ \mathbf{R}_1{}^{(i+1)}=\mathcal{H}\left\{\mathbf{X}^{(i+1)}\right\}-\mathbf{U}^{(i+1)}\mathbf{V}^{(i+1)H}+\mathbf{R}_1{}^{(i)}\\ \mathbf{R}_2{}^{(i+1)}=\mathcal{H}\left\{\mathbf{X}^{(i+1)}\right\}-\mathbf{U}^{(i+1)}\mathbf{V}^{(i+1)H}+\mathbf{R}_2{}^{(i)}\end{cases} \tag{18}$$

Specifically, the solution for $\mathbf{X}^{(i+1)}$ can be written as

$$\mathbf{X}^{(i+1)} = P_{\Omega}\left(\frac{\rho_1 \mathcal{H}^{\dagger}\{\mathbf{U}^{(i)}\mathbf{V}^{(i)H} - \mathbf{R}_1^{(i)}\} + \rho_2 G^{?}\{\mathbf{Z}^{(i)} - \mathbf{R}_2^{(i)}\}}{\rho_1 + \rho_2}\right) + P_{\Omega}(\mathbf{S}) \tag{19}$$

where, $P_{\Omega}(\cdot)$ is the projection operator on Ω. Let $\mathcal{H}^{\dagger}\{\cdot\}$ and $G^{\dagger}\{\cdot\}$ denote the adjoint operators corresponding to the matrix, which can be computed as follows [7]

$$\mathcal{H}^{\dagger} = \left(\mathcal{H}^{H}\mathcal{H}\right)^{-1}\mathcal{H}^{H} \tag{20}$$

$$G^{\dagger} = \left(G^{H}G\right)^{-1}G^{H} \tag{21}$$

The solution of $\mathbf{Z}^{(i+1)}$ is a classic nuclear norm optimization problem, which can be directly solved by using the singular value thresholding (SVT) algorithm as follows [11]

$$\mathbf{Z}^{(i+1)} = SVT_{\lambda/\rho_2}\left\{G(\mathbf{X}^{i+1}) - \mathbf{R}_2^{(i)}\right\} \tag{22}$$

where, $SVT_{\lambda/\rho_2}\{\cdot\}$ denotes the SVT operator with parameter λ/ρ_2, whose detailed derivation is provided in [12].

The iterative solutions of $\mathbf{U}^{(i+1)}$ and $\mathbf{V}^{(i+1)}$ are respectively given by

$$\mathbf{U}^{(i+1)} = \rho_1\left(\mathcal{H}\{\mathbf{X}^{(i+1)}\} + \mathbf{R}_1^{(i)}\right)\mathbf{V}^{(i)}\left(\mathbf{I} + \rho_1\mathbf{V}^{(i)H}\mathbf{V}^{(i)}\right)^{-1} \tag{23}$$

$$\mathbf{V}^{(i+1)} = \rho_1\left(\mathcal{H}\{\mathbf{X}^{(i+1)}\} + \mathbf{R}_1^{(i)}\right)\mathbf{U}^{(i+1)}\left(\mathbf{I} + \rho_1\mathbf{U}^{(i+1)H}\mathbf{U}^{(i+1)}\right)^{-1} \tag{24}$$

Based on (8) ~ (24), through multiple iterations, the complete $\mathbf{X}$ can be reconstructed from sparse observation data when certain termination conditions are met.

IV. Simulation Results

In this section, the simulation experiments is performed to evaluate sparse echo reconstruction of the proposed algorithm. The main simulation parameters of the radar and micro-motion are shown in Table I. In addition, additive Gaussian white noise is added to the echo signal, with a signal-to-noise ratio (SNR) of 15 dB. Two cases of data missing rates corresponding to RMS are considered: 0.3 and 0.5.

In the first part, we compare FA echoes with RMS echoes, including high-resolution range profiles (HRRP) and time-frequency distributions (TFD). From Fig. 3 (a) and Fig. 3 (c), it can be seen that the missing samples corresponding to RMS occur randomly throughout the observation interval. Comparing Fig. 3 (b) and Fig. 3 (d), we find that due to the disruption of the coherence of the echo signal by RMS, the TFD is defocused and broken, making it impossible to obtain valid time-frequency ridges.

In the second part, we present the sparse reconstruction results of the proposed algorithm under different missing rates. Although the correlation of echoes is affected by sparse

TABLE I THE MAIN PARAMETERS.

Item	Value
Carrier frequency f_c	10 GHz
Pulse repetition frequency (PRF)	250 Hz
Bandwidth	3.2 GHz
Observation time	2 s
Cone rotation period T_c	1 s
Spin period T_s	2 s
The data missing ratio ϑ	0.3/0.5

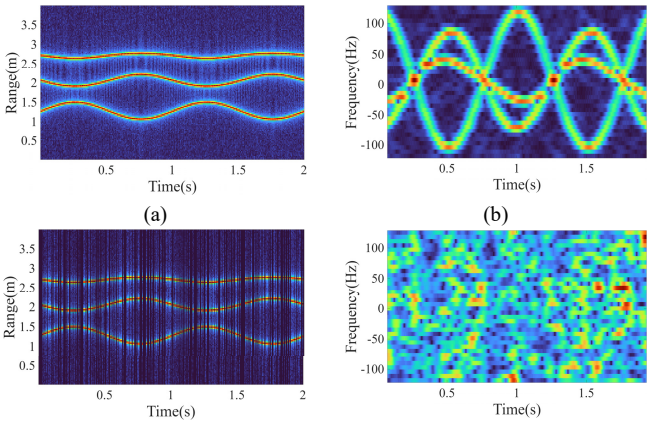

Fig. 3 Comparison of FA echo and RMS echo. (a) HRRP corresponding to FA. (b) TFD corresponding to FA. (c) HRRP corresponding to RMS ($\vartheta = 0.5$). (d) TFD corresponding to RMS ($\vartheta = 0.5$).

sampling, the corresponding autocorrelation functions can be located at the delay position corresponding to the cone rotation period at missing rates of $\vartheta = 0.3$ and $\vartheta = 0.5$, which is 250 time delays, as shown in Fig. 4. Based on the period estimation, the missing ridges corresponding to HRRP and TFD can be effectively recovered, achieving good reconstruction performance, as shown in Fig. 5. Comparing Fig. 3 (d) and Fig. 5 (d), the proposed algorithm can resolve the defocusing problem in TFD under the missing rate of $\vartheta = 0.5$, demonstrating the reliability of the proposed algorithm.

Finally, we present a comparison of reconstruction performance at missing time positions for different algorithms. We compared the proposed method, the MC method [6], the Modified Smoothed L0-norm (SL0) method [13], and the ground truth of the signal. Fig. 6 shows the estimation results of HRRP amplitude and HRRP phase reconstructed by different algorithms under the condition of $\vartheta = 0.5$. The Modified SL0 method, which belongs to a classical CS algorithm, relies solely on information from the slow-time dimension to recover the missing signals and consequently exhibits the poorest performance. Benefiting from the enhanced Hankel matrix, the proposed method and the MC method can fully leverage both the low-rank information from the fast-time and slow-time dimensions, leading to superior recovery performance. However, owing to the periodic constraint, the proposed method achieves a phase

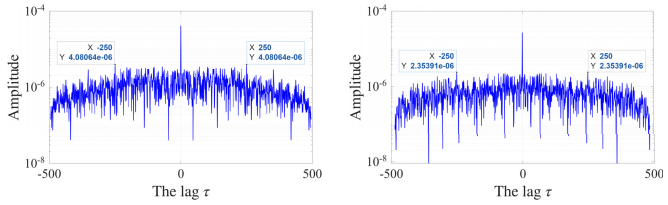

(a) (b)

Fig. 4 Autocorrelation functions of RMS echoes. (a) Autocorrelation function corresponding to $\vartheta = 0.3$. (b) Autocorrelation function corresponding to $\vartheta = 0.5$.

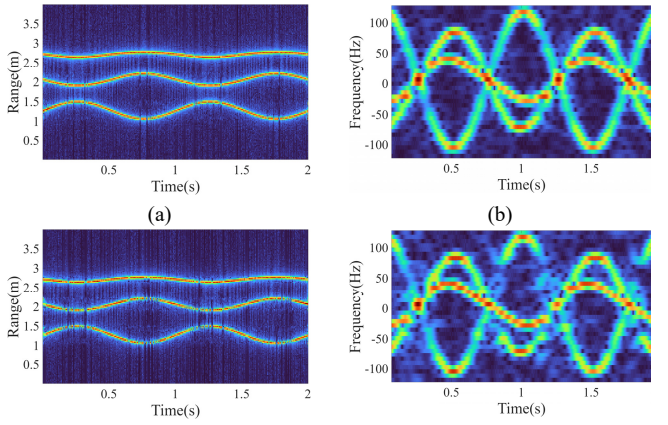

(a) (b)

(c) (d)

Fig. 5 Reconstruction results of HRRP and TFD. (a) Reconstructed HRRP at $\vartheta = 0.3$. (b) Reconstructed TFD at $\vartheta = 0.3$. (c) Reconstructed HRRP at $\vartheta = 0.5$. (d) Reconstructed TFD at $\vartheta = 0.5$.

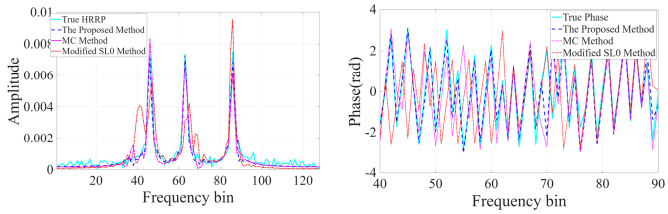

(a) (b)

Fig. 6 Performance comparison of different algorithms. (a) Reconstruction results of HRRP amplitude at the missing observation time. (b) Reconstruction results of HRRP phase at missing observation time.

reconstruction closer to the ground truth, demonstrating its superiority.

For quantitative evaluation, Table II presents the average computation time of different methods. All methods were implemented with MATLAB R2024a and run on a computer with an AMD Ryzen 5 7500F Central Processing Unit (CPU). It can be observed that the proposed method requires more computational time, primarily attributed to the large-dimensional expansion of the enhanced Hankel matrix. Additionally, the solution of $\mathbf{U}$ and $\mathbf{V}$ in (12) involves singular value decomposition (SVD). If $(M - 2P)(N - 2Q) < (2P + 1)(2Q + 1)$, the computational complexity of SVD is $O[(M-2P)^2(N-2Q)^2(2P+1)(2Q+1)]$, which contributes significantly to the computational overhead.

TABLE II RUNNING TIME COMPARISON.

Method	the MC method	The Modified SL0 method	the proposed method
Running time (s)	50.0742	7.0687	58.0320

V. CONCLUSIONS

To address sparse echo reconstruction for micro-motion targets under RMS, this paper proposes a sparse signal recovery method with joint low-rank and periodic consistency constraints. The periodic consistency regularization fully exploits similarity across micro-motion echoes. Experimental results demonstrate that our method effectively recovers signal information at missing positions and outperforms existing MC method. Future work will investigate robust period estimation for sparse signals to further enhance echo reconstruction performance. The future work will study the robust period estimation of sparse signals and reduce the complexity of the algorithm to further enhance echo reconstruction performance.

REFERENCES

[1] V. C. Chen, F. Li, S. Ho and H. Wechsler, "Micro-Doppler effect in radar: phenomenon, model, and simulation study," *IEEE Trans. Aerosp. Electron. Syst.*, vol. 42, no. 1, pp. 2-21, Jan. 2006.

[2] L. Liu, D. McLernon, M. Ghogho, W. Hu, and J. Huang, "Ballistic missile detection via micro-Doppler frequency estimation from radar return," *Digit. Signal Process.*, vol. 22, no. 1, pp. 87–95, Jan. 2012.

[3] Y. Kim and T. Moon, "Human detection and activity classification based on micro-Doppler signatures using deep convolutional neural networks," *IEEE Geosci. Remote Sens. Lett.*, vol. 13, no. 1, pp. 8–12, Jan. 2016.

[4] A. N. O'Donnell, J. L. Wilson, D. M. Koltenuk, and R. J. Burkholder, "Compressed sensing for radar signature analysis," *IEEE Trans. Aerosp. Electron. Syst.*, vol. 49, no. 4, pp. 2631–2639, Oct. 2013.

[5] L. Kang, B.-S. Liang, Y. Luo, and Q. Zhang, "Sparse imaging for spin ning space targets with short time observation," *IEEE Sensors J.*, vol. 21, no. 7, pp. 9090–9098, Apr. 2021.

[6] G. Xu, B. Zhang, J. Chen, F. Wu, J. Sheng, and W. Hong, "Sparse inverse synthetic aperture radar imaging using structured low-rank method," *IEEE Trans. Geosci. Remote Sens.*, vol. 60, pp. 1–12, 2021.

[7] J. Wang, M. Ding, and A. Yarovoy, "Interference mitigation for FMCW radar with sparse and low-rank Hankel matrix decomposi tion," *IEEE Trans. Signal Process.*, vol. 70, pp. 822–834, 2022.

[8] M. Jin, J. Wang, S. Wei, Z. Zeng, C. Zhang, and F. Qu, "Type parameter estimation of 2D-GTD model based on ADMM approach," *Electron. Lett.*, vol. 60, no. 10, May 2024, Art. no. e13216.

[9] D. Xu, H. Dong, C. Feng, and Z. Geng, "Translational motion compensation of ballistic target based on radon transform," *in Proc. 3rd IEEE Int. Conf. Comput. Commun.*, 2017, pp. 1707–1710.

[10] X. Bai, F. Zhou, M. Xing, and Z. Bao, "High-resolution radar imaging of air targets from sparse azimuth data," *IEEE Trans. Aerosp. Electron. Syst.*, vol. 48, no. 2, pp. 1643–1655, Apr. 2012.

[11] S. Zhang, Y. Liu, X. Li, and D. Hu, "Removal of micro-Doppler effect of ISAR image based on Laplacian regularized nonconvex low-rank representation," *IEEE Trans. Image Process.*, vol. 30, pp. 6446–6458, 2021.

[12] J. F. Cai, E. J. Candès, and Z. W. Shen, "A singular value threshold ing algorithm for matrix completion," *SIAM J. Optim.*, vol. 20, no. 4, pp. 1956–1982, Mar. 2010.

[13] L. Kang, B.-S. Liang, Y. Luo, and Q. Zhang, "Sparse imaging for spinning space targets with short time observation," *IEEE Sensors J.*, vol. 21, no. 7, pp. 9090–9098, Apr. 2021.